NANO LETTERS

2008
Vol. 8, No. 8
2277-2282

# Large Reversible Li Storage of Graphene Nanosheet Families for Use in Rechargeable Lithium Ion Batteries

**EunJoo Yoo,[†] Jedeok Kim,[‡] Eiji Hosono,[†] Hao-shen Zhou, Tetsuichi Kudo, and Itaru Honma*[,†]**

*Energy Technology Research Institute, National Institute of Advanced Industrial Science and Technology, Umezono 1-1-1, Central 2, Tsukuba, Ibaraki 305-8568 Japan; Nano Ionics Materials Group, National Institute of Materials Science, Namiki 1-1, Tsukuba, Ibaraki 305-0044 Japan*

*Received April 4, 2008; Revised Manuscript Received June 10, 2008*

## ABSTRACT

**The lithium storage properties of graphene nanosheet (GNS) materials as high capacity anode materials for rechargeable lithium secondary batteries (LIB) were investigated. Graphite is a practical anode material used for LIB, because of its capability for reversible lithium ion intercalation in the layered crystals, and the structural similarities of GNS to graphite may provide another type of intercalation anode compound. While the accommodation of lithium in these layered compounds is influenced by the layer spacing between the graphene nanosheets, control of the intergraphene sheet distance through interacting molecules such as carbon nanotubes (CNT) or fullerenes ($C_{60}$) might be crucial for enhancement of the storage capacity. The specific capacity of GNS was found to be 540 mAh/g, which is much larger than that of graphite, and this was increased up to 730 mAh/g and 784 mAh/g, respectively, by the incorporation of macromolecules of CNT and $C_{60}$ to the GNS.**

Graphene based materials are quite intriguing from both perspectives of fundamental science and technology, because they are nontoxic, chemically and thermally tolerant, electrically conductive, and mechanically hard. Such properties suggest a wide-range of industrial applications for graphene-based materials such as adsorbents, catalyst supports, thermal transport media, structural and electronic components, batteries/capacitors, and even application in biotechnology. In particular, advanced carbonaceous materials are desirable for use in energy technologies such as hydrogen storage, fuel cells, solar cells, lithium batteries, and capacitors, which have a strong requirement for superior storage devices. In state-of-the-art energy technologies, high-density lithium secondary batteries (LIB) are in high demand for electrical/hybrid vehicles, advanced electronics, and miscellaneous power devices.

Graphene nanosheets (GNS) are emerging nanomaterials that are two-dimensional layers with one-atomic thickness and strongly bonded carbon networks, which have attracted much interest for various applications of structural, thermal, electronic, and nanotechnologies.[1−12] In particular, these materials have superior electrical conductivities than graphitic carbon, high surface areas of over 2600 $m^2/g$, chemical tolerance, and a broad electrochemical window that would be very advantageous for application in energy technologies. The current electrode materials employed in LIB are lithium intercalation compounds such as graphite and $LiCoO_2$, because these materials can be reversibly charged/discharged under intercalation potentials with sufficient specific capacity. However, much higher density electrodes are increasingly important as the demand for advanced electrical vehicles and/or mobile electronic device power back-ups increases.

In this investigation, the possibility of higher lithium storage capacity was explored by controlling layered structures of graphene nanosheet (GNS) materials. The GNS materials can be prepared by exfoliation of a bulk graphite crystal to a dispersion of individual atomic-layer graphene sheets, and a reassembling process results in layered nanosheet products. According to this process, the nanosheet materials consist of numbers of atomic graphene sheets. Controlling the reassembling of monolayer graphene sheet materials in solution would allow the tuning of the inter layer spacing, the thickness of the GNS, and the morphology. Structural control of the nanosheet materials may affect the lithium storage properties. Functional nanocarbons such as carbon nanotubes (CNT) or fullerenes ($C_{60}$), which have been intensively investigated for advanced energy storage,[13−18] have been incorporated into the reassembling process of the GNS materials, identified here as GNS families, for the

* Corresponding author. Phone and fax: +81 298 61 5648. E-mail: i.homma@aist.go.jp.
[†] National Institute of Advanced Industrial Science and Technology.
[‡] National Institute of Materials Science.

10.1021/nl800957b CCC: $40.75 
**Published on Web 07/24/2008**

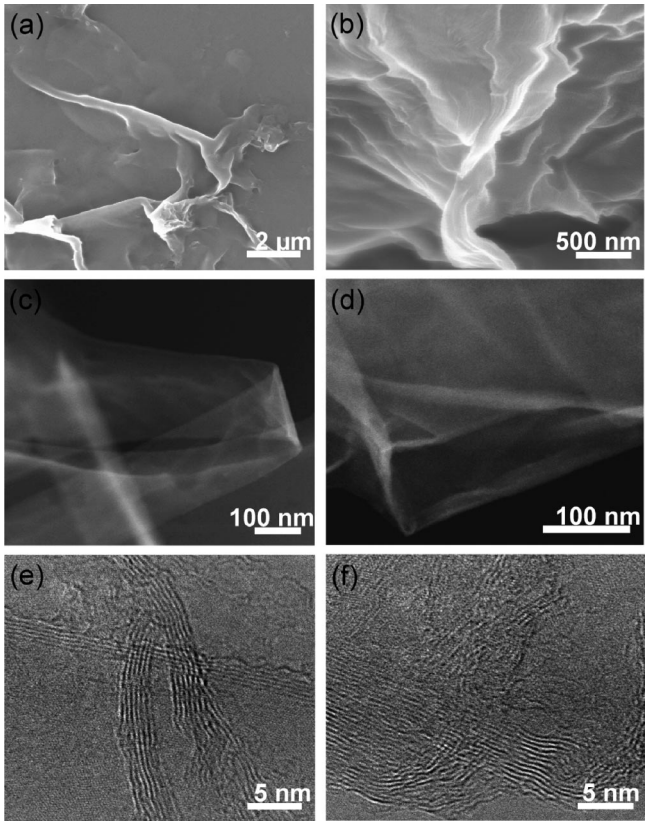


**Figure 1.** SEM and TEM observation of OGS and GNS. (a,b) SEM images of GNS. TEM images of (c) OGS and (d) GNS. (e,f) Cross-sectional TEM images of GNS.

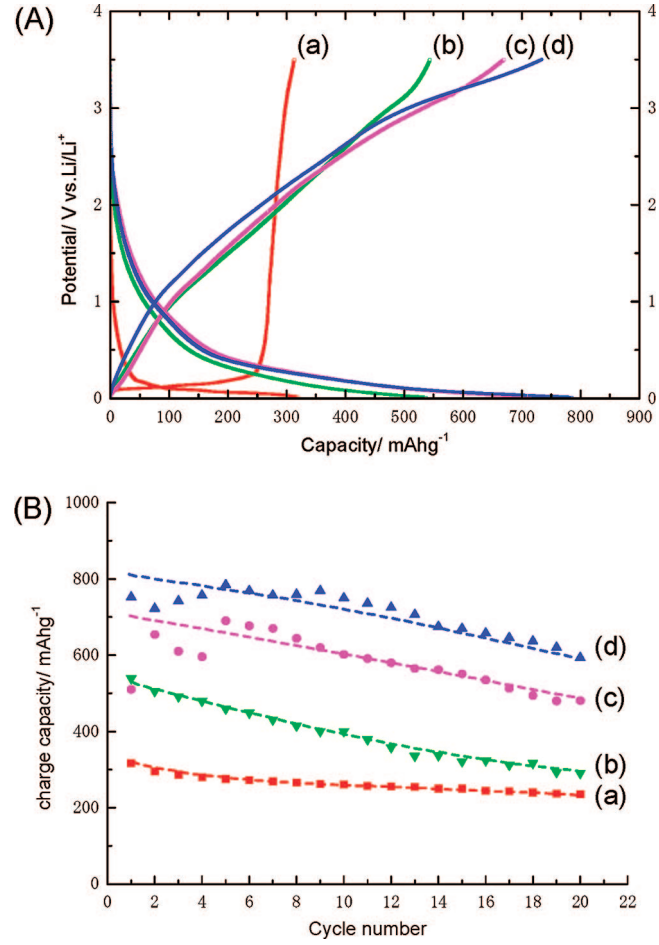


**Figure 2.** Lithium insertion/extraction properties of the GNS families. (A) charge/discharge profiles of (a) graphite, (b) GNS, (c) GNS+CNT, and (d) GNS+$C_{60}$ at a current density of 0.05 A/g. (B) Charge/discharge cycle performance of (a) graphite, (b) GNS, (c) GNS+CNT, and (d) GNS+$C_{60}$.

preparation of LIB intercalation anode materials. Enhancement of the specific capacity of these electrode materials, via interaction between the graphene nanosheet and the functional nanocarbons, was investigated with an aim to obtain an unusual nano-space size for lithium ion intercalation with higher energy densities.

TEM and SEM were used to characterize the structure of both the OGS and the reduced GNS materials. Figure 1a shows an SEM image of typical GNS, revealing a curled morphology consisting of a thin wrinkled paper-like structure. This structure suggests that the intrinsic ripples of GNS might develop into wavy structures in the macroscopic scale.[19,20] The thickness of the GNS can be observed in the magnified SEM image of Figure 1b. It was found that the graphene platelet thickness ranged from 3 to 7 nm, which corresponds to an approximately 10−20 layer stacking of the monatomic graphene sheets, according to an interlayer spacing of 0.335 nm for graphite. Figure 1c shows a TEM image of the typical OGS, and a curved monatomic nanosheet can be observed, suggesting that the oxidized graphene nanosheet has been fully exfoliated from the graphite by the process employed here. A monolayer of the oxidized graphene nanosheet (OGS) suggests a layer-by-layer exfoliation process of graphene monatomic sheets from the graphite. After reduction of the OGS, the GNS materials were formed and then characterized using TEM observation. Figure 1d shows a TEM image of the GNS, which shows a rippled and crumpled structure, similar to that of the original OGS. The similarity of the OGS and GNS sheet structures suggests that the in situ reduction reaction occurs in solution without disruption of the nanosheet morphology. Figure 1e,f shows the stacking sheet structure of GNS in the TEM cross sections, and individual monolayers of the GNS are clearly observed. The thickness of the GNS is approximately 2−5 nm and is composed of approximately 6−15 stacked individual monatomic graphene layers, which are clearly shown in the TEM cross sections. According to these figures, some parts of the GNS are wavy and turbostratic, indicating that the layer stacking is not commensurate and disordering, possibly because of the uncontrolled reassembling process of the nanosheet materials. Thus described, both the OGS and the GNS materials are nanosheet structured carbonaceous materials, synthesized from the layer-by-layer exfoliation of individual OGS, with a subsequent reduction process providing monatomic graphene sheets that are reassembled to form GNS structures with approximately 4 to 20 stacking layers.

The lithium insertion/extraction properties of graphite, GNS, GNS+CNT, and GNS+$C_{60}$ are shown in Figure 2. Figure 2A shows charge/discharge profiles for (a) graphite, (b) GNS, (c) GNS+CNT, and (d) GNS+$C_{60}$. Curve a shows the typical insertion/extraction properties expected for highly crystalline graphite electrode materials. A reversible capacity

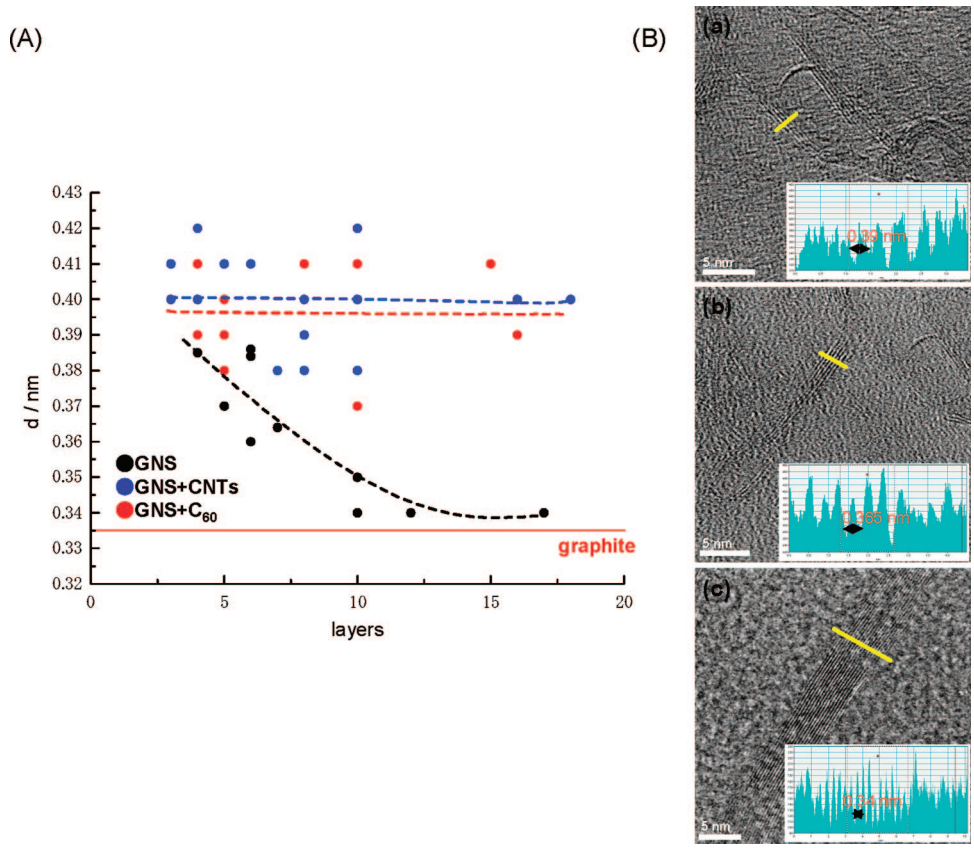


**Figure 3.** (A) Relationship between the number of graphene stacking sheets in the GNS families and the *d*-spacing perpendicular to the basal plane. (B) Cross-sectional TEM images of GNS with different numbers of graphene sheets: (a) 4 stacking layers, (b) 6 layers, and (c) 17 layers. The *d*-spacing increases as the layer number decreases.

of approximately 320 mAh/g was obtained at a current density of 0.05 A/g. In contrast, the charge/discharge curves of GNS, GNS+CNT, and GNS+$C_{60}$ displayed significantly different profiles compared with that of graphite, which indicates that the accommodation of lithium into these new classes of carbonaceous materials are different. For example, in the charging (insertion) curve, the slope starts approximately 2.5 V (vs Li/Li+) and has large specific capacities below 0.5 V without distinguishable plateaus. The profile implies the presence of at least two different Li-storage sites in GNS, GNS+CNT, and GNS+$C_{60}$. The capacity of the potential region lower than 0.5 V (vs Li/Li+) should be due to lithium intercalation into the graphene layers,[21] while the absence of a potential plateau suggests a disordered stacking of the graphene nanosheet structures, resulting in electrochemically and geometrically nonequivalent Li ion sites. Xue et al. suggested the Li ions are electrochemically adsorbed on both sides of single-layer sheets that are arranged like "falling cards".[22] However, the capacity above 0.5 V vs Li/$Li^+$, may be associated with a faradic capacitance either on the GNS surface or on the edge plane.[23] Similar Li-storage behavior can also be observed in hard carbon.[21,24] Furthermore, the reversible capacity at a current density of 0.05 A/g is 540, 730, and 784 mAh/g for GNS, GNS+CNT, and GNS+$C_{60}$, respectively. Obviously, the reversible capacity of the GNS, GNS+CNT, and GNS+$C_{60}$ families is much higher than that of the theoretical value of graphite (372 mAh/g). Yata et al. have reported that the accommodation of lithium in polyacenic semiconductors (PAS) up to the capacities of $LiC_2$ might be possible when the graphene layer distance is increased to approximately 0.4 nm.[25] The difference in the inter layer spacing between the PAS (0.4 nm) and the graphite (0.335 nm) is almost equal to the radius of a lithium ion (0.06 nm), which might provide a greater Li ion accommodation number than that of the limited $C_6Li$ stage 1 compounds.

Figure 2B shows a comparison of the charge/discharge cycle performance for (a) graphite, (b) GNS, (c) GNS+CNT, and (d) GNS+$C_{60}$. For the graphite material, the reversible capacity after 20 cycles was 240 mAh/g, or 78% retention of the initial capacity. However, the reversible capacity after 20 cycles was 290, 480, and 600 mAh/g for GNS, GNS+CNT, and GNS+$C_{60}$, respectively. The reversible retention capacity after 20 cycles was 54, 66, and 77% for GNS, GNS+CNT, and GNS+$C_{60}$, respectively. The data suggests that the fading capacity of GNS, GNS+CNT, and GNS+$C_{60}$ is somehow faster than that of the graphite; however, the large specific capacity of these materials suggests that lithium ions are reversibly inserted/extracted in the GNS by a similar intercalation mechanism to that occurring in graphite.

The theoretical limit of the specific capacity of a graphite electrode is considered to be 372 mAh/g, which corresponds to the composition of stage 1 Li-graphite intercalation compound (Li-GIC), that is, $C_6Li$.[26] However, as shown in Figure 2A, the charge/discharge capacities of GNS, GNS+CNT,

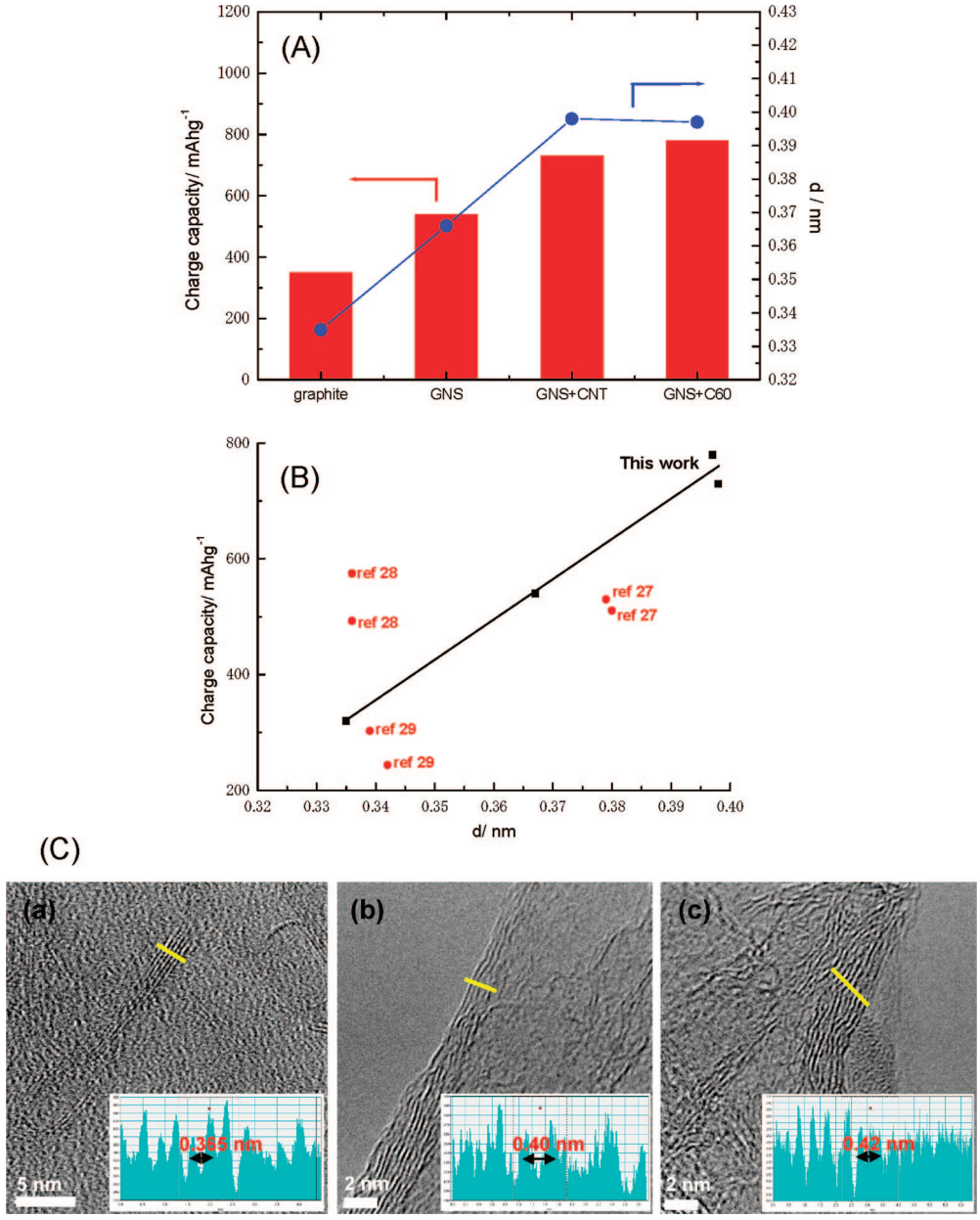


**Figure 4.** (A) Relationship between the *d*-spacing and the charge capacity of the GNS families and graphite. (B) Relationship between the *d*-spacing and the charge capacity of various reported carbonaceous nanomaterials, including the present work. (C) Cross-sectional TEM images of GNS families with almost the same numbers (5−6) of graphene stacking layers for (a) GNS, (b) GNS+CNT, and (c) GNS+$C_{60}$.

and GNS+$C_{60}$ are much higher than 372 mAh/g. This suggests that the formation of $LiC_6$ compound is not sufficient to explain such a high storage capacity. Consequently, other mechanisms for the storage of lithium ion species are required. In order to discuss the mechanism in detail, the detailed layered structures of the GNS families, GNS, GNS+CNT, and GNS+$C_{60}$, were investigated by TEM observation, as shown in Figure 3. Lithium storage in carbonaceous materials is strongly dependent on the nanostructure of the host material; therefore, it is very important to determine the phenomena occurring during the reassembling process and the associated structural changes of the GNS for accommodation of lithium ions. Figure 3A shows the relationship between the *d*-spacing and the graphene layer stacking number of the GNS families. Figure 3B shows cross-sectional TEM images of several GNS materials with different stacking numbers, and the direct line scanning analysis results of the lattice images perpendicular to the basal plane. According to this analysis, the layer-to-layer distance (*d*-spacing) can be measured. Pure GNS was found to possess a smaller average *d*-spacing of approximately 0.365 nm compared with those of GNS with CNT and $C_{60}$. Figure 3A shows that the *d*-spacing of the GNS changes with the stacking layer numbers, that is, the number of graphene layers accumulated to form the nanosheet material. Surprisingly, the *d*-spacing of GNS increased with the decrease in the number of graphene layers. The *d*-spacing of the GNS increases monotonically as the number of graphene layers is reduced; the *d*-spacing of the GNS with 17 stacking graphene layers is approximately 0.34 nm;

however, that with only 4 layers increases up to 0.385 nm. This indicates that the graphene intersheet distances are expanded by more than 9% by the reduction in the stacking layer numbers. The increased *d*-spacing of the GNS are displayed in the TEM images of Figure 3B, which shows the layer stacking of the nanosheet with enhanced intersheet distances. In contrast, the average *d*-spacing of the GNS+CNT and GNS+$C_{60}$ are approximately 0.40 nm, regardless of the stacking layer numbers, and are larger than that of GNS. The presence of the $\pi-$electron system macromolecules of CNT and $C_{60}$ must be responsible for the significant enhancement of the *d*-spacing in the GNS+CNT and GNS+$C_{60}$ structures.

Figure 4A shows the relationship between the *d*-spacing and the charge capacities for graphite and the GNS families. A trend of increasing reversible capacity was observed when the *d*-spacing of the material is increased. The average *d*-spacings of GNS, GNS+CNT, and GNS+$C_{60}$ are 0.365, 0.40, and 0.40 nm, respectively. The expansion ratio in the *d*-spacing is $(0.365 - 0.335/0.335) \times 100 = 9\%$ for GNS, and 19 and 19% for GNS+CNT and GNS+$C_{60}$, respectively. For GNS+$C_{60}$, with a *d*-spacing expanded by 19%, the reversible capacity was enhanced by 144% compared with that of graphite, from 320 to 784 mAh/g. Figure 4B shows the relationship between the charge capacity and the *d*-spacing of several carbonaceous materials including those in the present study. The expansion in *d*-spacing of the GNS families caused a linear increase of the specific capacity, while it is not so remarkable in the literatures.[27−29]

Figure 4C shows cross-sectional TEM images of GNS, GNS+CNT, and GNS+$C_{60}$, respectively, together with line analysis results of the stacking graphene layers. Comparison of the *d*-spacing for GNS, GNS+CNT, and GNS+$C_{60}$ with almost the same number of layers (5−6 layers) is shown. The *d*-spacing was found to be 0.365, 0.40, and 0.42 nm for GNS, GNS+CNT, and GNS+$C_{60}$, respectively, for a similar number of stacking graphene layers. It is considered that the addition of CNT and $C_{60}$ may cause an expansion of the *d*-spacing of the GNS material, possibly due to the electron affinity of both CNT and $C_{60}$.

Although the detailed lithium storage mechanisms are not clear for GNS, GNS+CNT, and GNS+$C_{60}$, it was found that the reversible capacity of GNS, GNS+CNT, and GNS+$C_{60}$ materials varied significantly depending on the *d*-spacing of the graphene nanosheet. Two possible reasons for the enhanced capacities of GNS, GNS+CNT, and GNS+$C_{60}$ can be proposed based on the different structures of graphite and GNS. First, the electronic structures of GNS, GNS+CNT, and GNS+$C_{60}$ must be different from that of graphite. Second, the expansion in the *d*-spacing of the graphene layers may cause additional sites for accommodation of lithium ions. Not only the regular sites of $C_6Li$, but also the next neighboring sites of stage 1 GIC compounds would be available because of both the structural and the electronic changes in the GNS materials. Therefore, these nanosheet forms of graphene are promising anode materials for future large-scale, high-capacity lithium ion batteries, although several problems remain to be solved before practical use in batteries can be realized. It was demonstrated that the *d*-spacing of GNS+CNT and GNS+$C_{60}$ are the largest (0.40 nm) compared with those of previous studies, as shown in Figure 4B, and this may be a crucial factor for large lithium reversible storage capacities in the GNS families up to 784 mAh/g. Further control of the reassembling process may provide an expansion of the interior space of the nanosheet compounds and three-dimensional morphologies, which may offer the promise of very large storage of lithium ions between graphitic carbon layers.

**Acknowledgment.** This work was supported by the New Energy and Industrial Technology Development Organization Japan under a grant for Research and Development of Nanodevices for Practical Utilization of Nanotechnology (Nanotech Challenge Project).

**Supporting Information Available:** Materials and methods, FT-IR spectra, X-ray diffraction patterns, Raman spectra, particle size distributions, TEM images, and charge/discharge profiles. This material is available free of charge via the Internet at http://pubs.acs.org.

## References

(1) Novoselov, K. S.; Geim, A. K.; Morozov, S. V.; Jiang, D.; Zhang, Y.; Dubonos, S. V.; Grigorieva, I. V.; Firsov, A. A. Electric Field Effect in Atomically Thin Carbon Films. *Science* **2004**, *306*, 666–669.
(2) Stankovich, S.; et al. Graphene-based composite materials. *Nature* **2006**, *442*, 282–286.
(3) Dikin, D. A.; et al. Preparation and characterization of graphene oxide paper. *Nature* **2007**, *448*, 457–460.
(4) Tombros, N.; Jozsa, C.; Popinciuc, M.; Jonkman, H. T.; van Wees, B. J. Electronic spin transport and spin precession in single graphene layers at room temperature. *Nature* **2007**, *448*, 571–575.
(5) Schedin, F.; Geim, A. K.; Morozov, S. V.; Hill, E. W.; Blake, P.; Katsnelson, M. I.; Novoselov, K. S. Detection of individual gas molecules adsorbed on graphene. *Nat. Mater.* **2007**, *6*, 652–655.
(6) Berger, C.; et al. Electronic Confinement and Coherence in Patterned Epitaxial Graphene. *Science* **2006**, *312*, 1191–1196.
(7) Cheianov, V. V.; Fal'ko, V.; Altshuler, B. L. The focusing of electron flow and a veselago lens in graphene pn junctions. *Science* **2007**, *315*, 1252–1255.
(8) Abanin, D. A.; Levitov, L. S. Quantized transport in graphene p-n junctions in a magnetic field. *Science* **2007**, *317*, 641–643.
(9) Miao, F.; Wijeratne, S.; Zhang, Y.; Coskun, U. C.; Bao, W.; Lau, C. N. Phase-coherent transport in graphene quantum billiards. *Science* **2007**, *317*, 1530–1533.
(10) Bunch, J. S.; et al. Electromechanical resonators from graphene sheets. *Science* **2007**, *315*, 490–493.
(11) Pisana, S.; Lazzeri, M.; Casiraghi, C.; Novoselov, K. S.; Geim, A. K.; Ferrari, A. C.; Mauri, F. Breakdown of the adiabatic Born-Oppenheimer approximation in graphene. *Nat. Mater.* **2007**, *6*, 198–201.
(12) Oostinga, J. B.; Heersche, H. B.; Liu, X.; Morpurgo, A.; Vandersypen, M. K. Gate-induced insulating state in bilayer graphene devices. *Nat. Mater.* **2008**, *7*, 151–157.
(13) Futaba, D. N.; Hata, K.; Yamada, T.; Hiraoka, T.; Hayamizu, Y.; Kakudate, Y.; Tanaike, O.; Hatori, H.; Yumura, M.; Iijima, S. Shape-engineerable and highly densely packed single-walled carbon nanotubes and their application as super-capacitor electrodes. *Nat. Mater.* **2006**, *5*, 987–994.
(14) Dai, G.-P.; Liu, C.; Wang, M.-Z.; Cheng, H.-M. Electrochemical Hydrogen storage behavior of ropes of aligned single-walled carbon nanotubes. *Nano Lett.* **2002**, *2*, 503–506.
(15) Kuc, A.; Zhechkov, L.; Patchkovskii, S.; Seifert, G.; Heine, T. Hydrogen sieving and storage in fullerene intercalated graphite. *Nano Lett.* **2007**, *7*, 1–5.
(16) Fang, B.; Zhou, H. S.; Honma, I. Ordered porous carbon with tailored pore size for electrochemical hydrogen storage application. *J. Phys. Chem. B* **2006**, *110*, 4875–7880.
(17) Fang, B.; Zhou, H. S.; Honma, I. Electrochemical hydrogen storage in Li-doped pentacene. *J. Chem. Phys. B* **2006**, *124*, 204718.

(18) Ishihara, T.; Kawahara, A.; Nishiguchi, H.; Yoshio, M.; Takita, Y. Effects of synthesis condition of graphitic nanocarbon tube on anodic property of Li-ion rechargeable battery. *J. Power Sources* **2001**, *97&98*, 129–132.
(19) Fasolino, A.; Los, J. H.; Katsnelson, M. I. Intrinsic ripples in graphene. *Nat. Mater.* **2007**, *6*, 858–861.
(20) Meyer, J. C.; Geim, A. K.; Katsnelson, M. I.; Novoselov, K. S.; Booth, T. J.; Roth, S. The structure of suspended graphene sheets. *Nature* **2007**, *446*, 60–63.
(21) Hu, J.; Li, H.; Huang, X. Electrochemical behavior and microstructure variation of hard carbon nano-spherules as anode materials for Li-ion batteries. *Solid State Ionics* **2007**, *178*, 265.
(22) Xue, J. S.; Dahn, J. R. Dramatic effect of oxidation on lithium insertion in carbons made from epoxy resins. *J. Electrochem. Soc.* **1995**, *142*, 3668.
(23) Yazami, R.; Deschamps, M. High reversible capacity carbon-lithium negative electrode in polymer electrolyte. *J. Power Sources* **1995**, *54*, 411.
(24) Ogumi, Z.; Inaba, M. Electrochemical lithium intercalation within carbonaceous materials: Intercalation Process, surface film formation, and lithium diffusion. *Bull. Chem. Soc. Jpn.* **1998**, *71*, 521.
(25) Yata, S.; Kinoshita, H.; Komori, M.; Ando, N.; Kashiwamura, T.; Harada, T.; Tanaka, K.; Yamabe, T. Structure and properties of deeply Li-doped polyacenic semiconductor materials beyond $C_6Li$ stage. *Synth. Met.* **1994**, *62*, 153.
(26) Tatsumi, K.; Iwashita, N.; Sakaebe, H.; Shioyama, H.; Higuchi, S.; Mabuchi, A.; Fujimoto, H. The influence of the graphitic structure on the electrochemical characteristics for the anode of secondary lithium batteries. *J. Electrochem. Soc.* **1995**, *3*, 716.
(27) Gotoh, K.; Maeda, M.; Nagai, A.; Goto, A.; Tansho, M.; Hashi, K.; Shimizu, T.; Ishida, H. Properties of a novel hard-carbon optimized to large size Li ion secondary battery studied by $^7$Li NMR. *J. Power Sources* **2006**, *162*, 1322.
(28) Yoo, S. H.; Park, C. W.; Yang, H.; Korai, Y.; Mochida, I.; Baker, R. T. K.; Rodriguez, N. M. Novel carbon nanofibers of high graphitization as anodic materials for lithium ion secondary batteries. *Carbon* **2004**, *42*, 21.
(29) Kawaguchi, M.; Imai, Y.; Kadowaki, N. Intercalation chemistry of graphite-like layered material $BC_6N$ for anode of Li ion battery. *J. Phys. Chem. Solids* **2006**, *67*, 1084.

NL800957B